NUMERICAL AND COMPUTATIONAL ANALYSIS OF HYDRODYNAMIC EFFECTS IN THE MICRO-HYDRO POWER STATION

Assoc.prof.dr. V. Bostan
Technical University of Moldova

INTRODUCTION

Among clean and non-pollutant energy sources, kinetic energy of the flowing rivers is of great importance due to the enormous energy potential. This assertion stands for the vast majority of rivers with large and medium size discharge. Strong public opposition to large scale hydro-electrical power plants caused by large environmental and social costs (from damming of rivers and flooding of large tracts of fertile land to the displacement of people from the affected areas and disrupted fish migration) is making the small scale hydro-electric power plants more appealing, especially for the potential consumers in remote rural areas. Micro-hydro-electric power plants are being used on a large scale as decentralized energy sources. Renewed interest for such stations started worldwide in recent decade.

Decentralized systems for conversion of the kinetic energy of the free water flow into electric or mechanical energy are using turbines in the absence of dams. The kinetic energy of free water flow is a recommended energy source available 24 hours per day and it can be efficiently harnessed by micro-hydro power stations. As working elements in such small-scale hydro-electric power stations are used Garman type rotors with oblique axis blades, Darrieus rotors, multi-blade rotors, Gorlov type turbines. There are two types of micro-hydro power stations without dams:

- anchored micro-hydro power stations;
- floating micro-hydro power stations.

The anchored power station requires a foundation to which the working elements, multiplicator and electric generator placed on a resistance frame are anchored. In contrast with anchored power stations, the floating micro-hydro power stations can be placed in the areas with higher flow rate and at further distances from the river banks. Moreover, they can be grouped and positioned appropriately to form a hydro power farm in order to convert more efficiently the flowing river kinetic energy. Nowadays, various types of floating micro-hydro power stations are being used with either horizontal or vertical axis.

Research and elaboration of the systems for conversion of renewable sources of energy (RSE) as a research objective, present interest and importance and it is in complete agreement with: European Union Strategy exposed in the White Book, commitments of the Republic of Moldova toward the increase of the RSE quote in the energy production up to 20% in 2020. The proposed innovations followed from a complex theoretical and experimental research in the context of which the rotor's geometrical, functional and constructive parameters have been argued and in a specialized laboratory with modern equipment the blade's fabrication technology using composite materials have been validated.

2. DETERMINATION OF HYDRODYNAMIC COEFFICIENTS C_L AND C_M

Consider the symmetrical profile of the blade placed in a uniform water stream with velocity $\vec{V}_\infty$ (fig. 1). In the fixing point O' of the symmetrical blade with lever OO' let consider three coordinate systems, namely: the $O'xy$ system with axis $O'y$ oriented in the direction of the velocity vector $\vec{V}_\infty$, and axis $O'x$ normal to this direction; the $O'x'y'$ system with axis $O'y'$ oriented along the lever direction OO', and axis $O'x'$ normal to this direction, and finally the $O'x''y''$ system with axis $O'x''$ oriented along the profile's chord toward the trailing edge and axis $O'y''$ normal to this direction . Points A and B correspond to the trailing and the leading edges, respectively. The angle of attack α is the angle between the profile's chord AB and the direction of the velocity vector $\vec{V}_\infty$, and the positioning angle φ is the angle formed by the velocity vector direction and lever OO'.

The hydrodynamic force $\vec{F}$ has its components in directions $O'x$ and $O'y$, named the lift and drag forces, respectively given by:

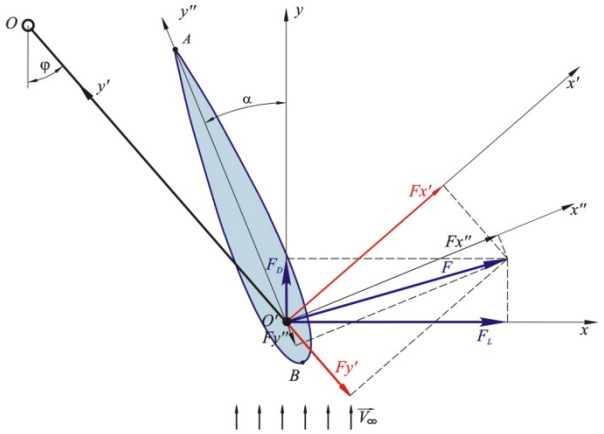

Figure 1. Hydrodynamic profile blade.

$$F_L = \frac{1}{2} C_L \rho V_\infty^2 S_p, \tag{1}$$

$$F_D = \frac{1}{2} C_D \rho V_\infty^2 S_p, \tag{2}$$

where ρ is the fluid density, V_∞ is the flow velocity, $S_p=ch$ (c is the length of chord AB, and h is the blade height) represents the lateral surface area of the blade, and C_L and C_D are dimensionless hydrodynamic coefficients, called the lift coefficient and drag coefficient. The hydrodynamic coefficients C_L and C_D are functions of the angle of attack α, the Reynolds number Re and the hydrodynamic shape of the blade profile. The pitching moment, is computed according to formula

$$M = \frac{1}{2} C_M \rho V_\infty^2 c S_p, \tag{3}$$

where C_M is the hydrodynamic moment coefficient.

The shape of the hydrodynamic profile is chosen from the library of *NACA* 4 digits aerodynamic profiles. The standard *NACA* 4 digit profiles are characterized by three shape parameters measured in percents of the chord's length: maximum value of camber C_{max}, location of the maximum camber $x_{C,max}$ and maximum thickness G_{max}. The profile coordinates are obtained by combining the camber line and the distribution of thickness [1]. Since the considered blades will have a symmetric shape, the camber is null ($C_{max}=0$, $x_{C,max}=0$) and the camber line will coincide with x-axis.

For simplicity, the profile chord length is considered unitary. Initially, the fluid is considered incompressible and inviscid, and its flow–plane and potential [3,4]. In the case of an incompressible plane potential flow the velocity components $\vec{V} = (u, v)$ in point $P(x,y)$ are given by the relations:

$$u(x,y) = \frac{\partial \Phi}{\partial x}, \; v(x,y) = \frac{\partial \Phi}{\partial y}, \tag{4}$$

where potential Φ is obtained by superposition of a uniform velocity flow and a distribution of sources and vortexes on the profile C. Thus, the potential is

$$\Phi = \Phi_\infty + \Phi_S + \Phi_V, \tag{5}$$

where the uniform flow potential is given by

$$\Phi_\infty = V_\infty x \cos\alpha + V_\infty y \sin\alpha, \tag{6}$$

the potential of the source distribution with strength $q(s)$ is

$$\Phi_S = \oint_C \frac{q(s)}{2\pi} \ln(r) ds, \tag{7}$$

and the potential of vortex distribution with strength $\gamma(s)$ is given by formula:

$$\Phi_V = -\oint_C \frac{\gamma(s)}{2\pi} \theta ds. \tag{8}$$

In relations (7,8) variable s represents the arc length along profile C, and (r,θ) are the polar coordinates of point $P'(x,y)$ relative to the point on the contour corresponding to arc length s (see fig.2).

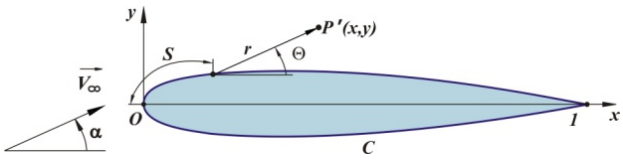

Figure 2. Potential two-dimensional flow around profile C.

Therefore the potential in point $P'(x,y)$ is computed as follows

$$\Phi(P') = V_\infty x \cos\alpha + V_\infty y \sin\alpha + \oint_C \frac{q(s)}{2\pi} \ln(r) ds - \oint_C \frac{\gamma(s)}{2\pi} \theta ds. \tag{9}$$

In order to compute the plane flow potential Φ the collocation method is used, that is: profile C is approximated by a closed polygonal line

$$C \approx \bigcup_{j=1}^{N} E_j,$$

with sides E_j having their vertices P_j and P_{j+1} on C. The vertices P_j are having a higher density near the leading and trailing edges. This is achieved by choosing Chebyshev points as their x-coordinates. Numbering of the vertices starts from the trailing

edge on the lower side in the direction of leading edge, passing further to the upper side (fig. 3).

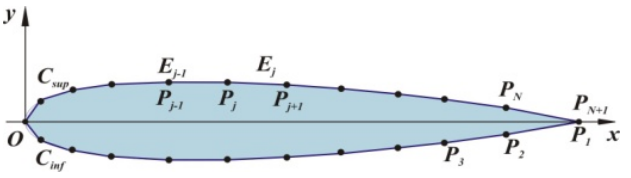

Figure 3. Discretization of profile C.

It is further assumed that the strength of vortexes $\gamma(s)$ distributed on profile C is constant on the boundary having value γ, and the strength of sources $q(s)$ distributed on the profile is piecewise constant on each boundary element E_j with value q_j, $j=1,...,N$. Breaking the integrals in equation (9) along each panel gives:

$$\Phi = V_\infty x\cos\alpha + V_\infty y\sin\alpha + \sum_{j=1}^{N}\int_{E_j}\left(\frac{q_j}{2\pi}\ln(r) - \frac{\gamma}{2\pi}\theta\right)ds \tag{10}$$

with unknowns γ and q_j, $j=1,\ldots,N$.

Consider now the boundary element E_j with vertices P_j and P_{j+1}. The unit normal and tangent vectors of the element E_j are given by:

$$\begin{aligned} n_j &= (-\sin\theta_j, \cos\theta_j), \\ \tau_j &= (\cos\theta_j, \sin\theta_j), \end{aligned} \tag{11}$$

where $\sin\theta_j = \dfrac{y_{j+1}-y_j}{L_j}$ and $\cos\theta_j = \dfrac{x_{j+1}-x_j}{L_j}$.

The unknowns γ and q_j from relation (10) are determined from the boundary and Kutta conditions. The boundary condition is the flow tangency condition along the profile:

$$\vec{V}\cdot\vec{n} = 0 \tag{12}$$

Imposing condition (12) on collocation points $M_j\left(\bar{x}_j, \bar{y}_j\right)$ chosen to be the midpoints of E_j and denoting the velocity components in M_j by u_j and v_j, respectively, provides N algebraic relations:

$$-u_j\sin\theta_j + v_j\cos\theta_j = 0,\ \mathrm{j}=1,\ldots,N \tag{13}$$

The last relation is provided by Kutta condition:

$$\vec{V}\cdot\vec{\tau}\big|_{E_1} = \vec{V}\cdot\vec{\tau}\big|_{E_N}, \tag{14}$$

where $\vec{\tau}$ denotes the unit tangent vector of the boundary element. Kutta condition (14) becomes:

$$u_1\cos\theta_1 + v_1\sin\theta_1 = -u_N\cos\theta_N + v_N\sin\theta_N. \tag{15}$$

The velocity components in point M_i are determined by the contributions of velocities induced by sources and vortexes on each boundary element E_j:

$$\begin{aligned} u_i &= V_\infty\cos\alpha + \sum_{j=1}^{N}u_{ij}^s q_j + \sum_{j=1}^{N}u_{ij}^v\gamma, \\ v_i &= V_\infty\sin\alpha + \sum_{j=1}^{N}v_{ij}^s q_j + \sum_{j=1}^{N}v_{ij}^v\gamma, \end{aligned} \tag{16}$$

where $u_{ij}^s, v_{ij}^s, u_{ij}^v, v_{ij}^v$ are the influence coefficients.

Let β_{ij}, $i\neq j$, be the angle between P_jM_i and M_iP_{j+1}, and set $\beta_{ii}=\pi$. Let $r_{ij} = dist(M_i, P_j)$ and define $D_{ij} = \dfrac{r_{i,j+1}}{r_{ij}}$, $i,j=1,\ldots,N$. It can be shown that the influence coefficients can be computed by the following formulas:

$$\begin{aligned} u_{ij}^s &= \frac{1}{2\pi}\left(-\ln D_{ij}\cos\theta_j - \beta_{ij}\sin\theta_j\right), \\ v_{ij}^s &= \frac{1}{2\pi}\left(-\ln D_{ij}\sin\theta_j + \beta_{ij}\cos\theta_j\right), \\ u_{ij}^v &= \frac{1}{2\pi}\left(-\ln D_{ij}\sin\theta_j + \beta_{ij}\cos\theta_j\right), \\ v_{ij}^v &= \frac{1}{2\pi}\left(\ln D_{ij}\cos\theta_j + \beta_{ij}\sin\theta_j\right), \end{aligned} \tag{17}$$

Substitute equations (16) and (17) in (13) and (15) to obtain a linear system with $N+1$ equations and $N+1$ unknowns γ and q_j, $j=1,...,N$ is obtained:

$$\left[A_{ij}\right]_{i,j=1}^{N+1}\begin{bmatrix} q_1 \\ q_2 \\ \vdots \\ q_N \\ \gamma \end{bmatrix} = \begin{bmatrix} b_1 \\ b_2 \\ \vdots \\ b_N \\ b_{N+1} \end{bmatrix}. \tag{18}$$

Coefficients A_{ij} and b_i are given by formulas:

$$A_{ij} = \frac{1}{2\pi}\left(\sin\Delta_{ij}\ln D_{ij} + \beta_{ij}\cos\Delta_{ij}\right),\ \ i,j=1,\ldots,N,$$

$$A_{i,N+1} = \frac{1}{2\pi}\sum_{j=1}^{N}\left(\cos\Delta_{ij}\ln D_{ij} - \beta_{ij}\sin\Delta_{ij}\right),\ \ i=1,\ldots,N,$$

$$A_{N+1,j} = \frac{1}{2\pi}\left(\beta_{1,j}\sin\Delta_{1j} + \beta_{N,j}\sin\Delta_{Nj} - \cos\Delta_{1j}\ln D_{1j} - \cos\Delta_{Nj}\ln D_{N,j}\right),$$

$$A_{N+1,N+1} = \frac{1}{2\pi}\sum_{j=1}^{N}\left(\sin\Delta_{1j}\ln D_{1j} + \sin\Delta_{Nj}\ln D_{N,j} + \beta_{1j}\cos\Delta_{1j} + \beta_{Nj}\cos\Delta_{Nj}\right),$$

$$b_i = V_\infty\sin\left(\theta_i - \alpha\right),\ \ i=1,\ldots,N,$$

$$b_{N+1} = -V_\infty\cos(\theta_1 - \alpha) - V_\infty\sin(\theta_N - \alpha)$$

with $\Delta_{ij} = \theta_i - \theta_j$.

The solution of linear system (18) provides the values of γ and q_j, using which the tangential components of velocity are computed:

$$u_{\tau i} = u_i \cos\theta_i + v_i \sin\theta_i.$$

Substitute (16) in the above relation to obtain:

$$u_{\tau i} = \left(V_\infty \cos\alpha + \sum_{j=1}^{N} u_{ij}^s q_j + \sum_{j=1}^{N} u_{ij}^v \gamma \right) \cos\theta_i + \left(V_\infty \sin\alpha + \sum_{j=1}^{N} v_{ij}^s q_j + \sum_{i=1}^{N} v_{ij}^v \gamma \right) \sin\theta_i.$$

Using (17) and algebraic manipulations obtain:

$$u_{\tau i} = \cos(\theta_i - \alpha) V_\infty + \frac{1}{2\pi} \sum_{j=1}^{N} \left(q_i \left(\beta_{ij} \sin\Delta_{ij} - \cos\Delta_{ij} \ln D_{ij} \right) + \gamma \left(\sin\Delta_{ij} \ln D_{ij} - \beta_{ij} \cos\Delta_{ij} \right) \right). \quad (19)$$

The local pressure coefficient on the discretized profile can be computed from relation

$$C_{p,i} = 1 - \left(\frac{u_{\tau i}}{V_\infty} \right)^2, \quad (20)$$

where $u_{\tau i}$ are given by (19). The hydrodynamic forces acting on the boundary element E_j and pitching moment coefficient are given by:

$$f_{xj} = C_{p,j} \left(y_{j+1} - y_j \right), \quad f_{yj} = C_{p,j} \left(x_{j+1} - x_j \right), \quad (21)$$

$$c_{m,j} = -f_{xj} \left(\frac{y_{j+1} - y_j}{2} \right) + f_{yj} \left(\frac{x_{j+1} - x_j}{2} - \frac{c}{4} \right). \quad (22)$$

The total force is the sum of contributions of each boundary element:

$$F_x = \sum_{j=1}^{N} f_{xj}, \; F_y = \sum_{j=1}^{N} f_{yj}, \quad (23)$$

Lift and moment coefficients are given by:

$$C_L = -F_x \sin\alpha + F_y \cos\alpha, \quad (24)$$

$$C_M = \sum_{j=1}^{N} c_{m,j}. \quad (25)$$

3. DETERMINATION OF HYDRODYNAMIC DRAG COEFFICIENT C_D

After the computation of the velocity distribution in the potential flow around the profile, next phase consists in the computation of boundary layer parameters divided into two sub-steps: laminar boundary layer and turbulent boundary layer [5-7]. The boundary layer starts at the stagnation point and follows the profile along the upper or lower surface in the direction of trailing edge, (fig.4).

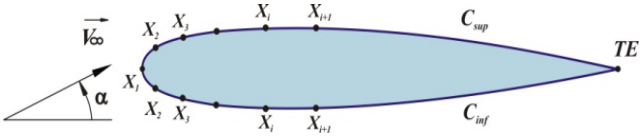

Figure 4. Profile discretization for boundary layer analysis.

The computation of laminar boundary layer parameters is based on the integral momentum and kinetic energy equations. The boundary layer thickness is defined as the distance from the profile at which the flow velocity differs by 1% from the velocity corresponding to the potential flow. Prandtl laminar boundary layer equations are derived from the steady incompressible Navier-Stokes equations:

$$\frac{\partial u}{\partial x} + \frac{\partial v}{\partial y} = 0, \quad \rho \left(u \frac{\partial u}{\partial x} + v \frac{\partial v}{\partial y} \right) = -\frac{\partial p}{\partial x} + \mu \frac{\partial^2 u}{\partial y^2}, \quad \frac{\partial p}{\partial y} = 0. \quad (26)$$

Here, x represents the measured distance along the contour from the stagnation point, and y is the measured distance in the normal to surface direction (fig. 5).

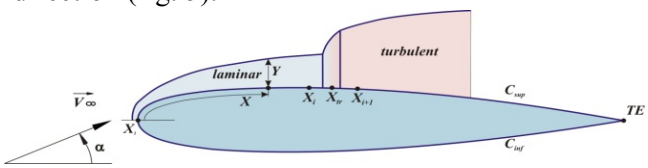

Figure 5. Transition from laminar to turbulent boundary layer.

Introduce the displacement thickness δ^*:

$$\delta^* = \int_0^\infty \left(1 - \frac{u}{V} \right) dy, \quad (27)$$

where V represents the velocity of the boundary layer exterior part in the considered point, and u is the tangential velocity in this point. Similarly, the momentum thickness θ is defined by

$$\theta = \int_0^\infty \left(1 - \frac{u}{V} \right) \frac{u}{V} dy, \quad (28)$$

and the kinetic energy thickness θ^* is given by

$$\theta^* = \int_0^\infty \left(1 - \frac{u^2}{V^2}\right)\frac{u}{V}dy. \quad (29)$$

By integrating equations (26) and using relations (27−29), the Von Karman integral-differential momentum equation is obtained

$$\frac{d\theta}{dx} + \frac{\theta}{V}\left(2 + \frac{\delta^*}{\theta}\right)\frac{dV}{dx} = \frac{1}{2}C_f, \quad (30)$$

where C_f denotes the local friction coefficient on the profile surface. Introduce the shape parameter

$$H = \frac{\delta^*}{\theta}. \quad (31)$$

Then, equation (30) can be rewritten as follows:

$$\frac{d\theta}{dx} + (2+H)\frac{\theta}{V}\frac{dV}{dx} = \frac{1}{2}C_f. \quad (32)$$

Multiply equation (30) by u and integrate it:

$$\frac{d\theta^*}{dx} + 3\frac{\theta^*}{V}\frac{dV}{dx} = 2C_d, \quad (33)$$

where C_d is the dissipation coefficient. Introduce the second shape parameter:

$$H^* = \frac{\theta^*}{\theta}. \quad (34)$$

Subtract equation (32) from equation (34) to get:

$$\theta\frac{dH^*}{dx} + H^*(H-1)\frac{\theta}{V}\frac{dV}{dx} = 2C_d - \frac{1}{2}H^*C_f. \quad (35)$$

The system of equations (32) and (35) is not sufficient to determine all unknowns. The additional relations are based on Falkner-Skan semi-empirical relations [6]. Assume the following correlation between H^* and H:

$$H^* = \begin{cases} 0.076\dfrac{(H-4)^2}{H} + 1.515, & \text{if } H < 4, \\ 0.04\dfrac{(H-4)^2}{H} + 1.515, & \text{otherwise.} \end{cases} \quad (36)$$

Also let $\mathrm{Re}_\theta = \mathrm{Re}\cdot\theta\cdot V$ and assume that

$$\frac{1}{2}\mathrm{Re}_\theta C_f = F_1(H),\ 2\mathrm{Re}_\theta\frac{C_d}{H^*} = F_2(H),$$

where

$$F_1(H) = \begin{cases} 0.01977\dfrac{(H-7.4)^2}{H-1} - 0.067, & \text{if } H < 7.4, \\ 0.022\dfrac{(H-7.4)^2}{(H-6)^2} - 0.067, & \text{otherwise,} \end{cases} \quad (37)$$

$$F_2(H) = \begin{cases} 0.00205(4-H)^{11/2} + 0.207, & \text{if } H < 4, \\ \dfrac{-0.003(H-4)^2}{1+0.02(H-4)^2} + 0.207, & \text{otherwise.} \end{cases} \quad (38)$$

Multiply equation (32) by Re_θ and let $\omega = (\mathrm{Re}_\theta)^2$

$$\frac{1}{2}V\frac{d\omega}{dx} + (2+H)\omega\frac{dV}{dx} = F_1(H). \quad (39)$$

Multiply (35) by Re_θ / H^* and rearrange terms:

$$\omega V\frac{d(\ln H^*)}{dH}\frac{dH}{dx} + (1-H)\omega\frac{dV}{dx} = F_2(H) - F_1(H). \quad (40)$$

Introduce the following notations:

$$A(x) = \frac{dV}{dx},\ F_3(H) = \frac{d(\ln H^*)}{dH},$$
$$F_4(H) = F_2(H) - F_1(H).$$

Then equations (39) and (40) are rewritten as follows

$$\begin{aligned} &\frac{1}{2}V(x)\frac{d\omega}{dx} + (2+H)\omega A(x) = F_1(H), \\ &\omega V(x)F_3(H)\frac{dH}{dx} + (1-H)\omega A(x) = F_4(H). \end{aligned} \quad (41)$$

The initial values are chosen to ensure that

$$\frac{dw}{dx}(0) = 0 \text{ and } \frac{dH}{dx}(0) = 0.$$

Therefore, *H(0)* is the solution of the following equation:

$$\frac{1-H}{2+H} = \frac{F_4(H)}{F_1(H)}.$$

Solving the above equation provides us the root $H(0) \approx 2.24$. Consequently,

$$\omega(0) = \frac{F_1(H(0))}{A(0)(2+H(0))}.$$

The initial conditions become

$$\begin{aligned} w(0) &= \frac{F_1(2.24)}{4.24A(0)}, \\ H(0) &= 2.24. \end{aligned} \quad (42)$$

The system of nonlinear ODE (41) with initial conditions (42) is solved by the Backward Euler method, but in order to avoid the implicit iterations at the transition from step j to step $j+1$ the functions F_1 and F_4 are linearized in the neighborhood of H_j, while F_3 takes the value $F_3(H_j)$. Thus, there is obtained a system of two bilinear equations with the unknowns H_{j+1} and ω_{j+1} :

$$A_j^1\omega_{j+1}+B_j^1H_{j+1}\omega_{j+1}+C_j^1H_{j+1}=D_j^1,$$
$$A_j^2\omega_{j+1}+B_j^2H_{j+1}\omega_{j+1}+C_j^2H_{j+1}=D_j^2, \quad (43)$$

where

$$A_j^1=\frac{V\left(x_{j+1}\right)}{2\Delta x}+2A\left(x_{j+1}\right),$$
$$B_j^1=A\left(x_{j+1}\right),$$
$$C_j^1=-F_1'\left(x_j\right),$$
$$D_j^1=\frac{V\left(x_{j+1}\right)}{2\Delta x}\omega_j+F_1\left(x_j\right)-F_1'\left(x_j\right)H_j=0,$$
$$A_j^2=A\left(x_{j+1}\right)-\frac{F_3(x_j)H_jV\left(x_{j+1}\right)}{\Delta x},$$
$$B_j^2=\frac{F_3(x_j)V\left(x_{j+1}\right)}{\Delta x}-A\left(x_{j+1}\right),$$
$$C_j^2=-F_4'\left(x_j\right),$$
$$D_j^1=F_4\left(x_j\right)-F_4'\left(x_j\right)H_j.$$

This method is iterated till either the transition from the laminar layer to the turbulent layer is predicted or trailing edge *TE* is reached.

The transition from laminar to turbulent boundary layer is located by Michel criterion, [7]. Let $\mathrm{Re}_x=\mathrm{Re}Vx$ and

$$\mathrm{Re}_{\theta\max}=1.174\left(1+\frac{22.4}{\mathrm{Re}_x}\right)\mathrm{Re}_x^{0.46}. \quad (44)$$

Then, transition takes place if $\mathrm{Re}_\theta>\mathrm{Re}_{\theta\max}$. Transition point is the root of the linear interpolation of $\mathrm{Re}_\theta(x)-\mathrm{Re}_{\theta\max}(x)$.

To analyze the turbulent boundary layer introduce the mean values and fluctuations:

$$\bar{q}(x,y)=\lim_{T\to\infty}\frac{1}{T}\int_{t_0}^{t_0+T}q(x,y,t)dt, \quad (45)$$
$$q'(x,y,t)=q(x,y,t)-\bar{q}(x,y). \quad (46)$$

The equations of the turbulent boundary layer are obtained from the Navier-Stokes equations:

$$\frac{\partial\bar{u}}{\partial x}+\frac{\partial\bar{v}}{\partial y}=0,$$
$$\rho\left(\bar{u}\frac{\partial\bar{u}}{\partial x}+\bar{v}\frac{\partial\bar{v}}{\partial y}\right)=-\frac{\partial\bar{p}}{\partial x}+\frac{\partial}{\partial y}\left(\mu\frac{\partial\bar{u}}{\partial y}-\rho\overline{u'v'}\right), \quad (47)$$
$$\frac{\partial\bar{p}}{\partial y}=\frac{\partial}{\partial y}\left(\mu\frac{\partial\bar{v}}{\partial y}-\rho\overline{v'^2}\right).$$

Similarly to the case of laminar boundary layer, the Von Karman integral equations are obtained. The computations of the turbulent boundary layer parameters are done by applying the Head's model [6]. Consider the flow volume in the boundary layer at an arbitrary point *x*:

$$Q(x)=\int_0^{\delta(x)}udy.$$

Then the displacement thickness is given by:

$$\delta^*=\delta-\frac{Q}{V}.$$

Introduce the entrainment velocity:

$$E=\frac{d}{dx}(V\theta H_1).$$

According to the Head's model the dimensionless velocity *E/V* depends only on H_1, and H_1, in its turn, depends only on *H*. Cebeci and Bradshow [6] have considered the empirical relations

$$\frac{E}{V}=0.0306(H_1-3)^{-0.6169} \quad (48)$$

and consequently

$$H_1=\begin{cases}0.8234(H-1.1)^{-1.287}+3.3, & H\le 1.6,\\ 1.5501(H-0.6778)^{-3.064}+3.3, & \text{otherwise.}\end{cases} \quad (49)$$

Finally, the last equation to determine the unknowns θ, H, H_1 and C_f is the Ludwieg-Tillman wall friction law:

$$C_f=\frac{0.246}{10^{0.678H}\,\mathrm{Re}_\theta^{0.268}}. \quad (50)$$

Combine the Von Karman integral equation and the relations (48)–(50) to obtain the following ODE system:

$$\frac{dY}{dx}=g(Y,x), \quad (51)$$

where $Y=\begin{bmatrix}\theta & H_1\end{bmatrix}^T$, and

$$g(Y,x)=\begin{bmatrix}-\dfrac{\theta\left(H_1+2\right)}{V}\dfrac{dV}{dx}+\dfrac{1}{2}C_f\\ -\dfrac{H_1}{V}\dfrac{dV}{dx}-\dfrac{H_1}{\theta}\dfrac{d\theta}{dx}+\dfrac{0.0306}{\theta\left(H_1-3\right)^{0.6169}}\end{bmatrix}.$$

The initial values are the final values supplied by the laminar boundary layer step. The numerical integration of system (51) is done by Runge-Kutta method of order 2, namely:

$$Y^*=Y_j+h_jg(Y_j,x_j),$$
$$Y_{j+1}=Y_j+h_j\left(\frac{1}{2}g(Y_j,x_j)+\frac{1}{2}g(Y^*,x_j)\right).$$

The calculation is done either till the trailing edge is reached or till the separation of the turbulent layer occurs.

Squire-Young formula [8] is applied to compute the drag coefficient C_D:

$$C_D = 2\left(\theta V^{\lambda}|_{x_{TE},C_{upper}} + \theta V^{\lambda}|_{x_{TE},C_{lower}}\right), \qquad (52)$$

where $\lambda = \left(H|_{x_{TE}} + 5\right)/2$.

4. THE TORQUE AND THE FORCES ACTING ON THE MULTI-BLADE HYDRAULIC ROTOR

The numerical methods, described previously, are used to compute the hydrodynamic coefficients $C_{L,ref}$ and $C_{D,ref}$ for the symmetrical profiles selected from the *NACA* library of aerodynamic profiles with a reference chord length $c_{ref}=1m$. Fig. 6 shows the hydrodynamic lift $C_{L,ref}$ and drag $C_{D,ref}$ coefficients. Taking into account the data from Fig. 6, the *NACA 0016* hydrodynamic profile is being selected as the reference profile.

The numerical methods, described previously, are used to compute the hydrodynamic coefficients corresponding to NACA 0016 profile with the chord length $c_{ref} = 1\,m$: $C_{L,ref}, C_{M,ref}$ and $C_{D,ref}$ by formulas (24), (25) and (52). The coefficients corresponding to the profile with the chord length *1.3 m* are calculated from the relations:

$$\begin{aligned} C_L &= 1.3 C_{L,ref}, \\ C_M &= (1.3)^2 C_{M,ref}, \\ C_D &= 1.3 C_{D,ref}. \end{aligned} \qquad (53)$$

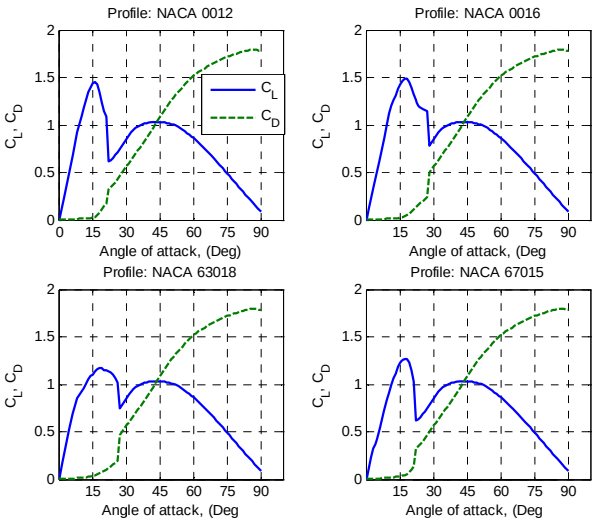

Figure 6. Hydrodynamic lift C_L and drag C_D coefficients versus the angle of attack for NACA 0012, 0016, 63018 and 67015 profiles.

The working angle of attack is selected to be $\alpha = 18^{o}$. During a full revolution around the rotor's axis the blade changes its attack angle depending on its position (fig. 7). Thus, in sector I the angle of attack (angle formed by the blade's chord and water flow direction) is 18˚; in sector II the angle of attack shifts from 18˚ up to -18˚, but the blade does not contribute to the total torque developed at the rotor shaft. In this sector, extended up to approximately 60˚, the blade is carried freely by the water flow and its re-positioning ends with an angle of attack of -18˚ at the end of sector III. The angle of attack is -18˚ in sector III. In sectors IV-VI the hydrodynamic effect is minimal and the blade has to be re-positioned from angle -18˚ to angle 18. In order to use the kinetic energy in the sectors IV-VI it is proposed to re-position the blade from -18˚ to 90˚ in sector IV; in sector V the blade remains under an angle of 90˚, and in sector VI the angle of attack returns to 18˚.

The magnitude of the hydrodynamic force $\overline{F}$ acting on the blade, and its tangential and normal components F_x and F_y versus the positioning angle are presented in fig. 8.

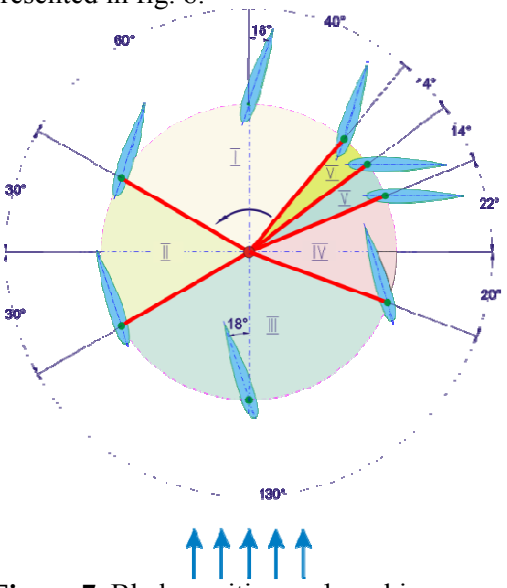

Figure 7. Blade position and working areas.

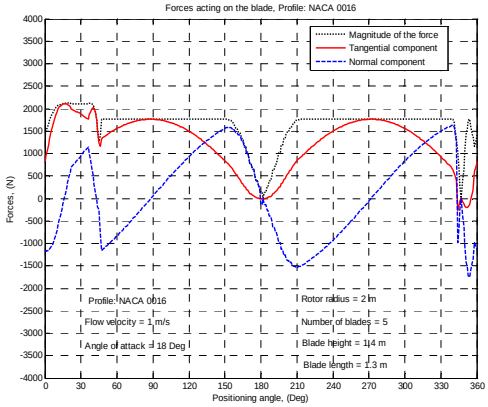

Figure 8. Magnitude, tangential component and normal component of the hydrodynamic force of a rotor blade versus the positioning angle.

Fig. 9 shows the torque $T_{r,i}$ developed by a single blade versus the positioning angle. Fig. 10 shows the total torque at the rotor shaft $T_{r\Sigma}$ developed by all blades versus the positioning angle. Fig. 11 shows the total torque $T_{r\Sigma}$ for three water flow velocities V_∞.

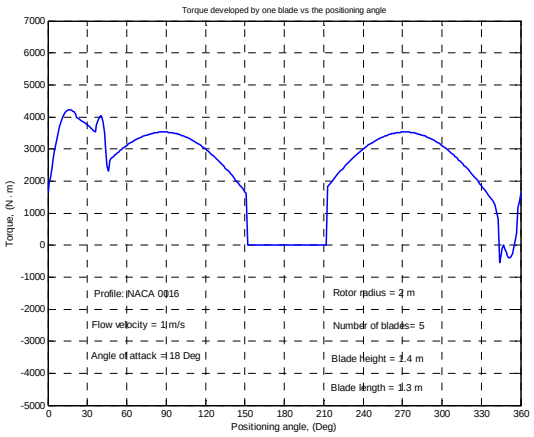

Figure 9. Torque $T_{r,i}$ developed by the rotor blade versus the positioning angle.

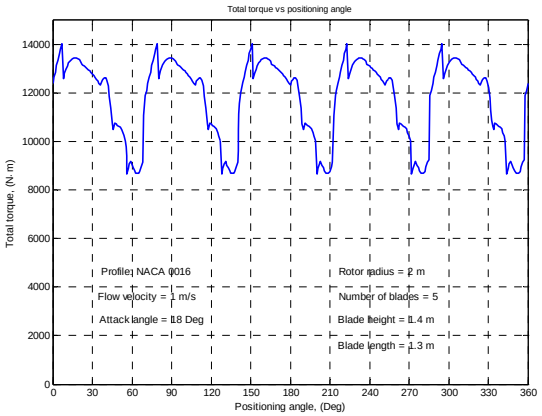

Figure 10. Total torque $T_{r\Sigma}$ developed by 5 blades at rotor shaft versus the positioning angle.

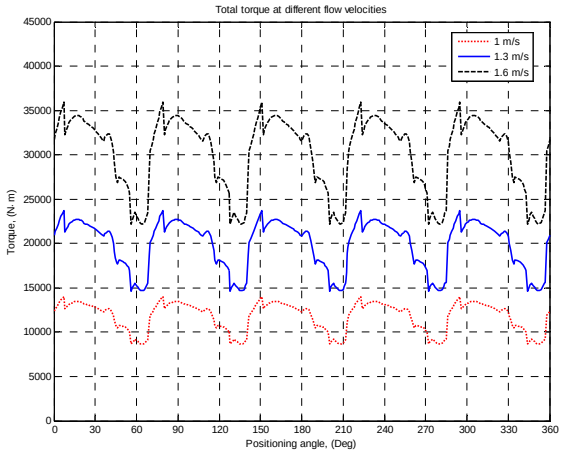

Figure 11. Total torque $T_{r\Sigma}$ at rotor shaft versus the positioning angle for various water flow velocities.

To determine the optimal working angle of attack it is necessary to compute the value of the torque developed by one blade and the total torque for several values of the angle of attack, namely: $\alpha = 15^o,\ 17^o,\ 18^o,\ 20^o$, (fig. 12−13).

Also, the performance of 3-, 4- and 5-blades rotor was analyzed. The total moment developed by the rotor shaft was computed and the results are presented in fig. 14.

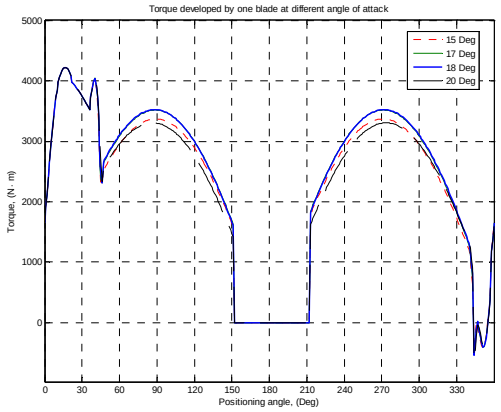

Figure 12. Torque $T_{r,i}$ developed by one blade versus the positioning angle.

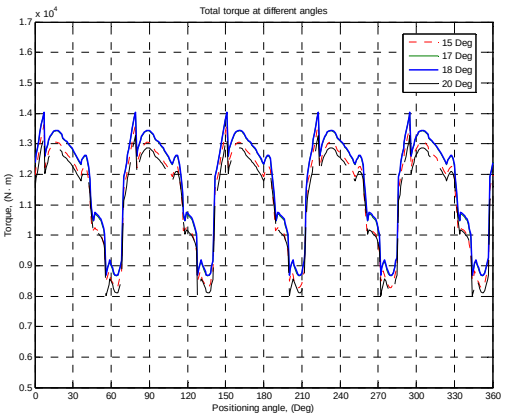

Figure 13. Total torque $T_{r\Sigma}$ developed by 5 blades versus the positioning angle.

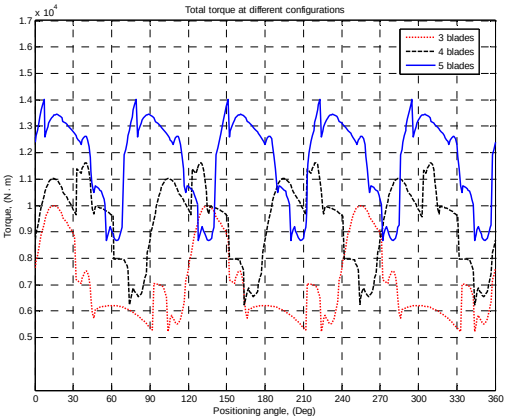

Figure 14. Total torque $T_{r\Sigma}$ developed at the 3-, 4- and 5-blade rotor shaft versus the positioning angle.

5. OPTIMIZATION OF NACA 0016 PROFILE

In order to maximize the torque produced by the micro hydro power plant rotor, the optimization of the hydrodynamic profile will be considered. The torque depends on the lift and drag hydrodynamic forces. The hydrodynamic forces through the hydrodynamic coefficients depend on the angle of attack α, Reynolds number Re and the shape of the hydrodynamic profile. The hydrodynamic shape of the profile was selected from the NACA library of profiles having as parameter only the maximal thickness. The angle of attack constitutes the second parameter. The optimization aims at maximizing the lift force and, at the same time, does not allow the pitching moment and the drag force to take very large values. The following optimization problem is considered:

$$\text{Maximize } C_L = C_L(\theta,\alpha)$$

subject to constraints on C_D and C_M,

where θ is the maximum thickness and α is the angle of attack. The negative maximum value for the moment coefficient will correspond to the solution for the angle of attack 0^o. The maximum value for the drag coefficient will correspond to the solution for the angle of attack $\alpha = 18^\circ$. Also, restrictions have been added to the optimization

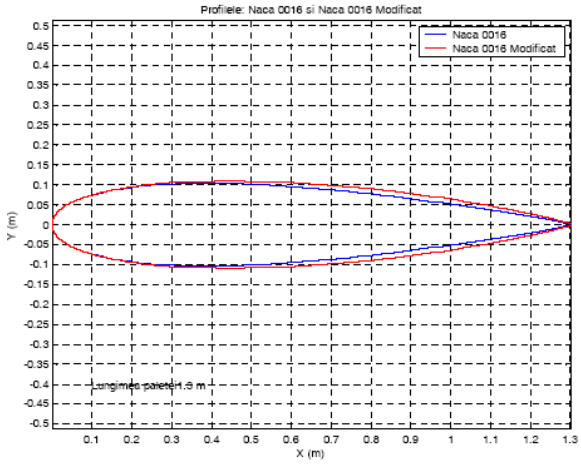

Figure 15. Standard and optimised NACA 0016 hydrodynamic profile.

parameters $10\% \le \theta \le 20\%$ and $0^o \le \alpha \le 20^o$. The following method is used:

While given accuracy is not attained do,

Solve $B_i s_i = -\nabla f(x_i)$,

$x_{i+1} = x_i + \alpha_i s_i$,

End do

where α_i are the multipliers and B_i are the positive definite approximations of the Hessian. The optimization is implemented in MATLAB with a sequential quadratic programming algorithm with a line search and a BFGS Hessian update. The quadratic sub-tasks are solved by modified projection method. The gradient of function $C_L = C_L(\theta,\alpha)$ is approximated with finite differences with uniform step $h = 10^{-4}$. NACA 0016 profile was considered as initial profile. The result of the shape optimization procedure is presented in fig. 15.

6. SIMULATION OF FLOW INTERACTION WITH HYDRODYNAMIC BLADES

In order to perform the deformation and stress analysis of a submersed blade with NACA 0016 hydrodynamic profile, the finite element ANSYS software is being used [13,14]. Consider a submersed blade in the water flow subjected to hydrodynamic forces corresponding to the flow velocity of 2 m/s and hydrostatic pressure. The maximum value of the forces acting on the blade is 11 KN.

The considered hydrodynamic blade has 5 transversal stiffening ribs made of aluminium alloy H37 with Young modulus $E = 1.97 \cdot 10^{11}\ N/m^2$ and Poisson coefficient $\nu = 0.27$,[12]. Due to the fact that the blades will be acting in aggressive conditions (water and possible debris), an important issue consists in the assurance of the blades impermeability. Thus, the hydrofoil is injected with polyurethane foam with density 0.6 kg/cm^3, $E = 0.95GPa$, $\nu = 0.24$. Blade's cover is made from multilayer composite material, fig. 16.

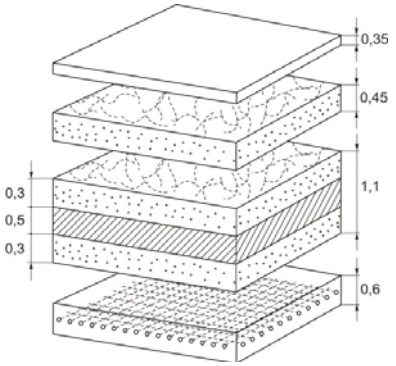

Figure 16. The structure of the composite material blade cover.

The Young modulus and Poisson coefficient are computed as [11], $E = 13.2GPa$ and $\nu_{12} = 0.3$.

Since the estimated deformations are small, the linear elasticity framework and Kirchhoff-Love

thin shell theory is adopted,[10]. Only the section between last two stiffening ribs is modelled. Discretization of the blade cover with Solsh190 for cover and Solid45 elements for foam is presented in fig. 17. The ribs are not modelled since their deformations are negligible and the constraints on the degrees of freedom are imposed: on line *A* (fig. 17) $u_x=0$, $u_y=0$ and $u_z=0$; on line B, $u_x=0$ and $u_y=0$; on line *C*, $u_z=0$.

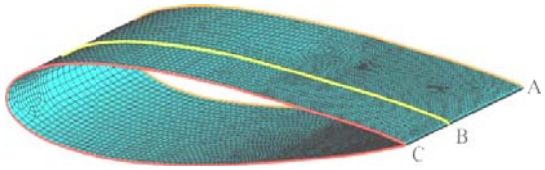

Figure 17. Discretization of the blade cover with Solsh190 finite elements.

In fig. 18, there are presented displacements in the injected with polyurethane foam blade with the same thickness of lateral cover: u_x (a), u_y (b) and u_z (c), with maximal displacement 0.01mm. Fig. 19 shows the main stresses in a blade injected with polyurethane foam: σ_1 (a), σ_2 (b) and σ_3 (c) (Pa).

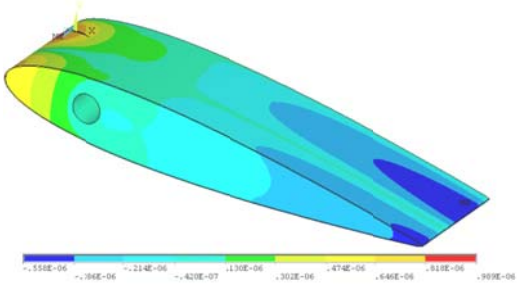

a.

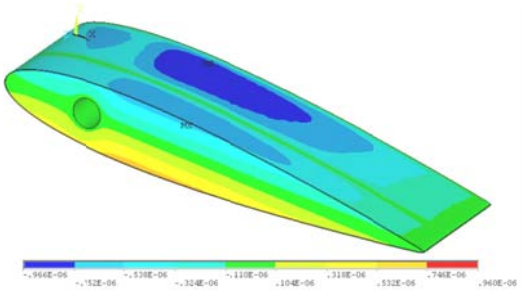

b.

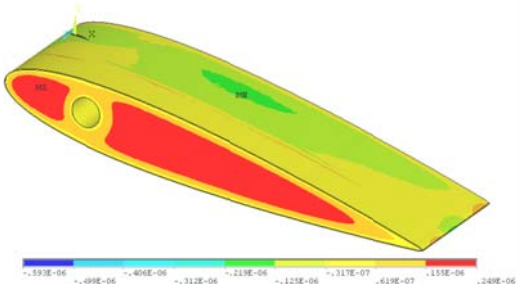

c.

Figure 18. Displacements in the blade: u_x (a), u_y (b) and u_z (c).

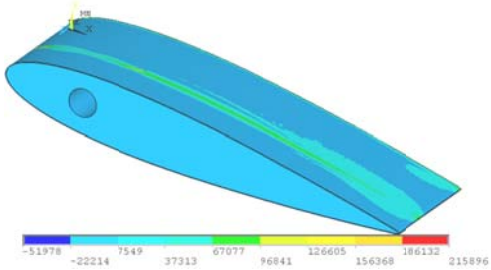

a.

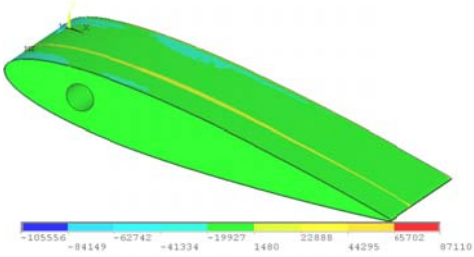

b.

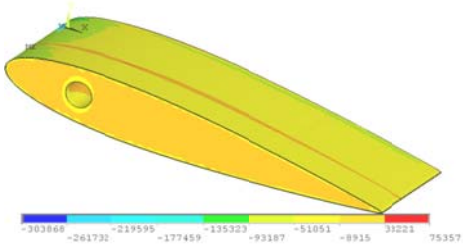

c.

Figure 19. Main stresses in the blade: σ_1 (a), σ_2 (b) and σ_3 (c) (Pa).

Modern technology for blade manufacturing from composite materials reinforced with fiberglass was developed. The developed technology comprises the following basic steps:

- design and manufacturing of the hydrodynamic profile moulding for the blade cover;
- elaboration of blade resistance structure;
- step-by-step layer shaping of the composite material;
- moulding of composite material coating, of resistance structure and injection with polyurethane foam.

The construction of the blade resistance structure complies with the manufacturing technology of the hydrodynamic blade cover with its partition along the symmetry axis. This allows the use of a single mould for the manufacturing of both parts of the blade cover. This constructive configuration of the blades ensures material savings and demands reduced labour force ensuring the manufacturing quality of the blade and complying with the geometrical parameters obtained from the theoretical calculation. The hydraulic turbines with 3 and 5 hydrodynamic blades have been manufactured at Centre for Renewable Energy Conversion Systems Design of the Technical University of Moldova.

7. FLOATABLE MICRO HYDROPOWER STATIONS

Based on carried out research, there have been elaborated two typo-dimensions of hydraulic turbines with 3 and 5 blades and optimal orientation of the blades with respect to the water stream direction. There were proposed [2], four different configurations of floatable micro hydropower stations for conversion of river kinetic energy into electric or mechanic energy.

Fig. 20 presents the kinematic scheme of the micro hydropower station MHCF D4x1,5M with 5 blades used for water pumping. In fig. 21, there is presented the constructive concept of micro hydropower station for electric energy generation MHCF D4x1,5E based on the hydraulic turbine with 5 blades. The blades 1 are mounted with bearings in rotor 2 coupled through a planetary gear 3 with electric generator 4. On the floating bodies 5 it is placed the spatial truss 7 coupled with the blades guiding and orientation mechanism 6.

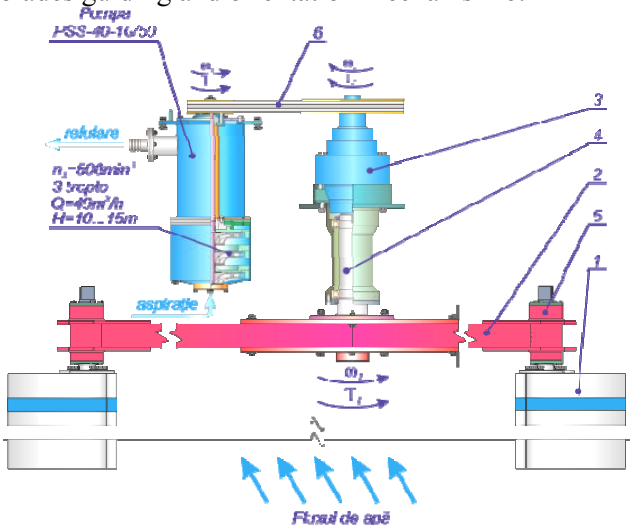

Figure 20. Kinematic scheme of a micro hydropower station: 1−blade, 2−rotor, 3−mechanical gear, 4,5− bearings, 6−belt drive.

Fig. 21 and 22 show the micro hydropower station MHCF D4x1,5E for the conversion of river kinetic energy into electric energy manufactured at industrial enterprises from Republic Moldova, and fig. 23 presents the micro hydropower station installed on river Prut.

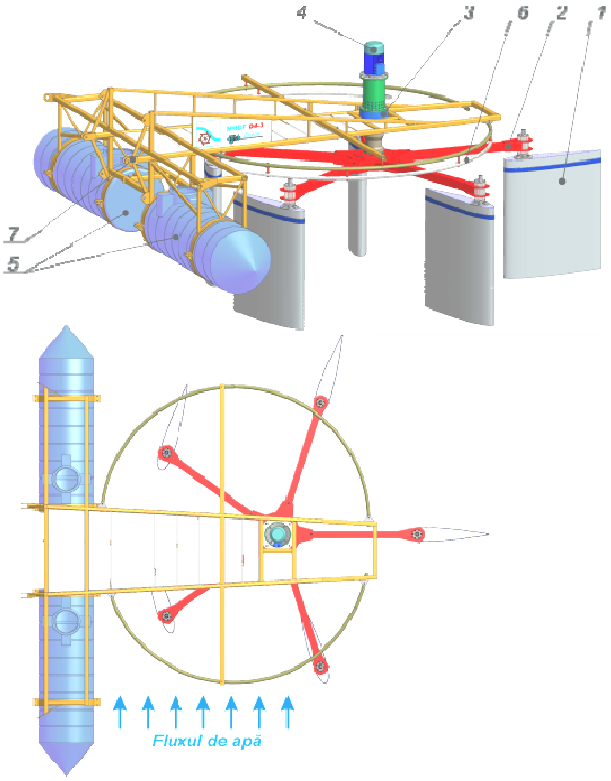

Figure 21. Micro hydropower station MHCF D4x1,5E.

Figure 22. Micro hydropower station MHCF D4x1,5E.

Figure 23. Micro hydropower station MHCF D4x1,5E installed on river Prut.

8. CONCLUSIONS

The hydraulic turbine with 5 hydrodynamic profile blades assures conversion of 49.5% of the energetic potential of water stream with velocity 1.3 m/s. The optimal orientation of the blades with respect to water stream direction (enabled by a guidance mechanism) assures participation of all blades (even those moving upstream) in generating the torque at the rotor shaft. The blades with composite materials cover injected with polyurethane foam and resistance structure with 5 stiffening ribs assure minimal local deformations that will not influence significantly the water flow and efficiency of energy conversion. Experimental testing of the micro hydropower station MHCF D4x1,5E in real field conditions confirmed that the hydropower station with hydrodynamic 5−blade rotor assures the conversion of the energy at the rotor shaft to the generator clams with efficiency of 77.5%.

References:

1. I. Bostan, V. Dulgheru, V. Bostan, R. Ciuperca. Anthology of Inventions: Systems for Renewable Energy Conversion. Ch.: "BonsOffices"SRL, 2009. 458pp. ISBN: 978-9975-80-283-3.

2. I. Bostan, V. Bostan, V. Dulgheru. Numerical modelling and simulation of the fluid flow action on rotor blades of the micro-hydropower station, Ovidius University Annals of Mechanical Engineering, Vol. VIII, Tom I, 2006, p.70-78.

3. J. Moran. An Introduction to Theoretical and Computational Aerodynamics, John Wiley and sons, 1984.

4. J. Katz, A. Plotkin. Low Speed Aerodynamics, From Wing Theory to Panel Methods, Mac-Graw Hill, 1991.

5. G.K. Batcelor. An Introduction to Fluid Dynamics, Cambridge University Press, 1970.

6. T. Cebeci, P. Bradshaw. Momentum Transfer in Boundary layers, Hemisphere Publishing Corportation, 1977.

7. W.C. Reynolds, T. Cebeci. Calculation of Turbulent Flows, Springer-Verlag, Topics in Applied Physics Series, Vol.12, 1978.

8. R.Michel. Etude de la Transition sur les Profiles d'Ales, Onera Report, 1/1578A, 1951.

9. H.B. Squire, A.D. Young. The Calculation of the Profile Drag of Aerofoils, R.&M.1838, ARC Technical Report , London, 1938.

10. P. G. Ciarlet. Mathematical Elasticity, vol.II. Theory of Plates, Elsevier Science B.V., Amsterdam, 1997.

11. R. M. Jones. Mechanics of Composite Materials, 2nd Edition, Taylor & Francis, 1999.

12. MIL-HDBK-17 Composite Materials Handbook.

13. ANSYS 10.0, User's Guide.

14. ANSYS 10.0, Advanced Analysis Techniques Guide

Recommended for publication 12.03.2012.